Revision 1

Te-rich raspite, $Pb(W_{0.56}Te_{0.44})O_4$, from Tombstone, Arizona, USA: the first natural example of Te^{6+} substitution for W^{6+}

Marcelo B. Andrade*, Hexiong Yang, Robert T. Downs, Robert A. Jenkins, and Isabel Fay

Department of Geosciences, University of Arizona, Tucson, Arizona 85721-0077, USA

* Present address: Department of Physics and Informatics, São Carlos Institute of Physics, University of São Paulo, Caixa Postal 369, 13560-970 São Carlos, SP, Brazil

Corresponding author: mabadean@terra.com.br

Abstract

Te-rich raspite, $Pb(W_{0.56}Te_{0.44})O_4$, from the Grand Central mine, Tombstone, Arizona, USA was studied with single-crystal X-ray diffraction, Raman spectroscopy, and electron microprobe analysis. The mineral represents the first natural example of Te^{6+} substitution for W^{6+}. It displays monoclinic symmetry with space group $P2_1/a$ and unit cell parameters a = 13.621(3), b = 5.019(1), c = 5.586(1) Å, β = 107.979(5)°, and V = 363.2(2) $Å^3$. Its structure consists of distorted MO_6 (M = W + Te) octahedra sharing edges to form zigzag chains running parallel to [010]. These octahedral chains are linked together by seven coordinated Pb^{2+} cations. In addition, a refinement of the regular raspite structure with measured chemistry $Pb_{1.00}W_{1.00}O_4$, $P2_1/a$ symmetry and unit cell parameters a = 13.5773(8), b = 4.9806(3), c = 5.5670(3) Å, β = 107.658(3)°, and V = 358.72(4) $Å^3$ is presented. Compared to regular raspite ($PbWO_4$), the partial substitution of the small radius Te^{6+} for larger W^{6+} results in a decrease in the MO_6 octahedral distortion, with a concomitant increase in the MO_6 octahedral volume and the average Pb-O bond length. In addition, as should be expected for mixed occupancy compounds, most Raman bands for the mixed Te-rich raspite are broader than the corresponding ones for the end-member regular raspite. High-temperature annealing experiments reveal that Te-rich raspite transforms irreversibly to the stolzite structure at 590(10) °C, which is considerably higher than the reported transformation temperature of 395(5) °C for regular raspite.

Always consult and cite the final, published document. See http://www.minsocam.org or GeoscienceWorld

Revision 1

Keywords: Te-rich raspite, lead tungstate, stolzite, crystal structure, X-ray diffraction, Raman spectra, phase transformation

Introduction

Naturally occurring lead tungstate ($PbWO_4$), has been reported to crystallize as the high-temperature tetragonal $I4_1/a$ stolzite (Plakhov et al. 1970) or the low-temperature monoclinic $P2_1/a$ raspite (Fujita et al. 1977). These phases are useful as scintillators compounds and possesses many unique physical properties, such as high density, short radiation length, short decay constant, and rather high radiation hardness (e.g., Arora and Chudasama 2007; Yeom and Lim 2012). They have been used as laser host materials (Chen et al. 2001), scintillators in high-energy physics detectors (Kobayashi et al. 1998; Annenkov et al. 2002), and an oxide ion conductor (Takai et al. 1999). Furthermore, considerable efforts have been devoted to synthesize nanobelt or bamboo-leaf-like raspite to understand its luminescence properties (George et al. 2008; Zheng et al., 2010).

Relative to the tetragonal stolzite, the low-temperature monoclinic raspite is rather rare in nature and transforms irreversibly to stolzite between 400 and 450 °C (Shaw and Claringbull 1955; Bastians et al. 2004). In addition, a third monoclinic ($P2_1/n$) phase, $PbWO_4$-III, can be synthesized by quench from high-pressure and high-temperature conditions (Richter et al. 1976). Raspite was originally described by Hlawatsch (1897) from Broken Hill, New South Wales, Australia. Shaw and Claringbull (1955) conducted the first X-ray structural analysis on this mineral, but only located the positions of Pb^{2+} and W^{6+}. A detailed structural model of raspite was reported by Fujita et al. (1977) without anisotropic displacement parameters for O atoms ($R = 0.080$). This paper reports the structure determinations of a Te-rich raspite, $Pb(W_{0.56}Te_{0.44})O_4$, and a regular raspite of ideal composition $PbWO_4$, from single-crystal X-ray diffraction experiments along with Raman spectra measured before and after heat-treatments, revealing that the substitution of Te^{6+} for W^{6+} can appreciably expand the phase stability field of raspite as a function of temperature.

Experimental Procedures

Always consult and cite the final, published document. See http://www.minsocam.org or GeoscienceWorld

Revision 1

The Te-rich raspite specimen used in this study is from the Grand Central mine, Tombstone, Arizona, USA, and is in the collection of the RRUFF Project (http://rruff.info/R130514). The crystals are pale yellow-to-colorless, elongated, and prismatic-to-tabular. They are associated with chlorargyrite, emmonsite, ottoite, quartz, and jarosite. The regular raspite specimen is from Broken Hill, New South Wales, Australia (http://rruff.info/R050567) and the crystals display similar morphology to the Te-rich raspite. The chemical compositions of the two samples were analyzed using a Cameca SX100 electron microprobe at 20 kV and 20 nA with a beam size of < 1 μm. The following standards were used: NBS K458 glass (Pb), scheelite (W), zinc telluride (Te) and anorthite (Al). The average compositions (wt.%) (9 analysis points for both samples) are PbO 50.79(51), WO_3 30.93(1.55), TeO_3 18.26(1.75), and Al_2O_3 0.12(4) for Te-rich raspite, and PbO 48.85(28) and WO_3 50.93(32) for regular raspite. The resultant empirical formulas are $Pb_{0.96}(W_{0.57}Te_{0.44}Al_{0.01})_{1.02}O_4$ and $Pb_{1.00}W_{1.00}O_4$ for Te-rich and regular raspite, respectively.

Single-crystal X-ray diffraction data for Te-rich and regular raspite were collected from nearly equi-dimensional crystals on a Bruker X8 APEX2 CCD X-ray diffractometer equipped with graphite-monochromatized Mo*K*α radiation. Reflections with $I > 2\sigma(I)$ were indexed based on a monoclinic unit cell (Table 1). No satellite or super-lattice reflections were observed. The intensity data were corrected for X-ray absorption using the Bruker program SADABS. The systematic absence of reflections suggest the unique space group $P2_1/a$. The crystal structure was solved and refined using SHELX97 (Sheldrick 2008). The positions of all atoms were refined with anisotropic displacement parameters. For simplicity, during the Te-raspite structure refinements, the Pb site was assumed to be fully occupied by Pb and the M (= W + Te) site by (0.56 W + 0.44 Te). The Pb site occupancy was also varied during the refinement, which produced a refined occupancy of 1.01. A full Pb occupancy model was thus adopted. For the regular raspite, the structure refinement indicated the ideal formula $PbWO_4$. Final atomic coordinates and displacement parameters are listed in Table 2, and selected bond lengths and angles in Table 3.

The Raman spectra of Te-rich and regular raspite were recorded on randomly oriented crystals on a Thermo Almega microRaman system, using a solid-state laser with a

Always consult and cite the final, published document. See http://www.minsocam.org or GeoscienceWorld

Revision 1

frequency of 532 nm and a thermoelectrically cooled CCD detector. The laser is partially polarized with 4 cm^{-1} resolution and a spot size of 1 μm.

To better understand the effect of the Te^{6+} substitution for W^{6+} on the raspite-to-stolzite transformation, we also carried out high-temperature annealing experiments on both Te-rich and regular raspite. The two samples were heated at a series of increasing temperatures from 390 to 600 °C in air in 10 or 20 °C steps for 24 h duration at each temperature. Both samples were examined by Raman spectroscopy at each step after cooling to bracket the temperature ranges for the phase transformation.

Results and Discussion

Crystal Structure

The crystal structure of Te-rich raspite is characterized by distorted MO_6 (M = W + Te) octahedra sharing edges to form zigzag chains parallel to [010]. These octahedral chains are interlinked by Pb atoms coordinated to seven O atoms (Fig. 1, Table 3). Compared to the MO_6 octahedron in regular raspite, that in Te-rich raspite is noticeably less distorted, as measured by the octahedral angle variance (OAV) and quadratic elongation (OQE) indices (Robinson et al. 1971),85 and 1.029, respectively, for the MO_6 octahedron in Te-rich raspite and 104 and 1.038 for that in regular raspite (Table 3). The greater distortion of the MO_6 octahedron in regular raspite stems primarily from the so-called second order Jahn-Teller (SOJT) effect of W^{6+}, owing to its empty *d*-shell (e.g., Ra et al. 2003; Lufaso and Woodward 2004). In contrast, Te^{6+} has a full *d*-shell, which suppresses part of the SOJT distortions.

The partial substitution of smaller Te^{6+} (r = 0.56 Å) for larger W^{6+} (r = 0.60 Å) (Shannon 1976) results in little change in the average *M*-O bond distance, but a significant increase in the average Pb-O bond length from 2.610 Å in regular raspite to 2.635 Å in Te-rich raspite (Table 3). Nevertheless, due to less distortion, the volume of the MO_6 octahedron in Te-rich raspite (9.472 $Å^3$) is larger than that in regular raspite (9.426 $Å^3$) (Table 3). Thus, it appears that the Te^{6+} substitution for W^{6+} in raspite reduces its structural packing efficiency, making the unit-cell parameters of Te-rich raspite greater than those of regular raspite (Table 1). Similar results have been observed for the $LaNi_{0.8}M_{0.2}O_3$ solid

Always consult and cite the final, published document. See http://www.minsocam.org or GeoscienceWorld

Revision 1

solution (M = Mo^{6+}, Te^{6+}, W^{6+}), in which the unit-cell volume of the Te-bearing phase is larger than that of the W-bearing phase (Alvarez et al. 1995, 1997).

From the crystal-chemical point of view, because six-coordinated W^{6+}, Mo^{6+}, and Te^{6+} have similar ionic radii, 0.60, 0.59, and 0.56 Å (Shannon 1976), respectively, one may expect extensive solid solutions among them. This is indeed the case for some synthetic compounds, such as $LaNi_{0.8}M_{0.2}O_3$ (M = Mo^{6+}, Te^{6+}, W^{6+}) (Alvarez et al. 1995, 1997), $Pb_2Mg(W_{1-x}Te_x)O_6$ (Rivezzi and Sciau 1998), $LiY(W_{1-x}Te_x)O_8$ (Wang et al. 2010), and a variety of Mo-Te mixed oxides used as catalysts in the gas phase selective oxidation of hydrocarbons (e.g., López Nieto et al. 2003; Holmberg et al. 2007; Botella et al. 2009). However, there has been no report thus far for the significant substitution of Te^{6+} for W^{6+} or Mo^{6+} in minerals, despite the common substitution between W^{6+} and Mo^{6+}, as in the scheelite group of minerals (Tyson et al. 1988, Zhang et al. 1998) and in stolzite from France (Chiappero et al. 2011). Therefore, our Te-rich raspite represents the first natural example of Te^{6+} substituting for W^{6+}.

Raman Spectra

Both raspite and stolzite have been previously investigated with Raman spectroscopy (Frost et al. 2004, Bastians et al. 2004; Yang and Huang 2012). Detailed assignments of major Raman bands for raspite have been proposed by Bastians et al. (2004). Figure 2 shows the Raman spectra of Te-rich and regular raspite. Evidently, the two spectra are analogous, but some differences between them are discernible. Specifically, as a consequence of the partial Te^{6+} substitution for W^{6+} (Te-W disordering) in the octahedral site, most Raman bands for Te-rich raspite are considerably broader than the corresponding ones for regular raspite. In particular, between 840 and 920 cm^{-1}, there is only one strong, sharp band at 870 cm^{-1} for regular raspite, which is ascribable to the W-O symmetrical stretching vibrations within the WO_6 octahedron (Bastians et al. 2004; Yang and Huang 2012). In contrast, there are two strong overlapped bands in the same region for Te-rich raspite, the major one at 881 cm^{-1} and the shoulder at 871 cm^{-1} (Fig. 2), which may be assigned to the Te-O and W-O symmetrical stretching vibrations within the MO_6 octahedron, respectively, as the Te-O bond is shorter and stronger with more covalent nature than the W-O bond (Wang et al. 2010). The bands between 620 and 750 cm^{-1} for the

Always consult and cite the final, published document. See http://www.minsocam.org or GeoscienceWorld

two minerals have been assigned to the *M*-O anti-symmetrical vibrations (Bastians et al. 2004; Yang and Huang 2012). Similarly, these bands are broader and more complex for Te-rich raspite than for regular raspite due to the partial Te^{6+} substitution for W^{6+}.

The irreversible transformation from the raspite to stolzite structure has been the subject of several investigations because it puts operational constraints on high-tech applications (Shaw and Claringbull, 1955; Bastians et al. 2004; Wang et al. 2010; Yang and Huang 2012). Te/W are tetrahedrally coordinated in stolzite, in contrast to six coordinated in raspite. Since the raspite to stolzite transformation is not reversible, our Raman spectra measured from the annealed samples indicate the temperatures at which the phase transformation occurred, which is 395(5) °C for regular raspite and 590(10) °C for Te-rich raspite (Fig. 3). The higher phase transition temperature for Te-rich raspite is a consequence of the stronger Te^{6+}-O bond compared to the weaker W^{6+}-O bond (Wang et al. 2010), thus requiring more energy to break. In other words, our data indicate that the phase stability field of raspite as a function of temperature can be markedly increased through the substitution of Te^{6+} for W^{6+}.

Acknowledgements

We are very grateful to Bruce Murphy for providing the Te-rich raspite sample to the RRUFF project. This study was supported by the Arizona Science Foundation and CNPq from the Brazilian government. We are also grateful to the reviewers for their valuable suggestions, which have improved the quality of our manuscript.

References cited

Annenkov, A.A., Korzhik, M.V., and Lecoq, P. (2002) Lead tungstate scintillation material. Nuclear Instruments and Methods in Physics Research, A490, 30-50.

Alvarez, I., Veiga, M.I., and Pico, C. (1995) Synthesis and structural characterization of a new perovskite series derived from $LaNiO_3$: $La_5Ni_4MO_{15}$ (M = Mo, Te, W). Journal of Materials Chemistry, 5, 1049-1051.

Always consult and cite the final, published document. See http://www.minsocam.org or GeoscienceWorld

Revision 1

Alvarez, I., Veiga, M.I., and Pico, C. (1997) Structural characterization and electronic properties of A-substituted $LaNi_{0.8}M_{0.2}O_3$ (A = Ca, Sr; M = Te, W) perovskites. Solid State Ionics, 93, 329-334.

Arora, S.K., and Chudasama, B. (2007) Flux Growth and Optoelectronic Study of $PbWO_4$ Single Crystals. Crystal Growth & Design, 7, 296-299.

Bastians, S., Crump, G., Griffith, W.P., and Withnall, R. (2004) Raspite and studtite: Raman spectra of two unique minerals. Journal of Raman Spectroscopy, 35, 726-731.

Botella, P., García-González, E., Solsona, B., Rodríguez-Castellón, E., González-Calbet, J.M., and López Nieto, J.M. (2009) Mo-containing tetragonal tungsten bronzes. The influence of tellurium on catalytic behaviour in selective oxidation of propene. Journal of Catalysis, 265, 43–53.

Chen, W., Inagawa, Y., Omatsu, T., Tateda, M., Takeuchi, N., and Usuki, Y. (2001) Diode-pumped, self-stimulating, passively Q-switched Nd^{3+}: $PbWO_4$ Raman laser. Optical Communications, 94, 401-407.

Chiappero, P.–J., Dietrich, J.E., Galvier, J., Gol, D., Merchadier, Y., Muller, E., and Bayle, L.-D. (2011) Stolzite from the Sainte Lucie mine, Lozere, France. Mieralogical Record, 42, 9-32.

Frost, R.L., Duong, L., and Weier, M. (2004) Raman microscopy of selected tungstate minerals. Spectrochimica Acta, A60, 1853-1859.

Fujita, T., Kawada, I., and Kato, K. (1977) Raspite from Broken Hill. Acta Crystallographica, B33, 162-164.

George, T., Joseph, S., Sunny, A.T., and Mathew, S. (2008) Fascinating morphologies of lead tungstate nanostructures by chimie douce approach. Journal of Nanoparticle Research, 10, 567-575.

Hlawatsch, C. (1897) Ueber den Stolzit und ein neues Mineral Raspit von Brokenhill, Annalen des K.K. Naturhistorischen Hofmuseums, 12, 33-41.

Holmberg, J., Wagner, J.B., Haggblad, R., Hansen, S., Wallenberg, L.R., and Andersson, A. (2007) Catalytic and structural effects of W-substitution in M2 Mo-V-Te-oxide for propene ammoxidation. Catalysis Today, 153–160.

Always consult and cite the final, published document. See http://www.minsocam.org or GeoscienceWorld

Revision 1

Kobayashi, M., Ishii, M., and Usuki, Y. (1998) Comparison of radiation damage in different $PbWO_4$ scintillating crystals. Nuclear Instruments and Methods in Physics Research, A406, 442-450.

López Nieto, J.M., Botella, P., Solsona, B., and Oliver, J.M. (2003) The selective oxidation of propane on Mo-V-Te-Nb-O catalysts: The influence of Te-precursor. Catalysis Today, 81, 87–94.

Lufaso, M.W., and Woodward, P.M. (2004) Jahn-Teller distortions, cation ordering and octahedral tilting in perovskites. Acta Crystallographica, B60, 10-20.

Plakhov, G.F., Pobedimskaya, E.A., Simonov, M.A., and Belov, N.V. (1970) The crystal structure of $PbWO_4$. Kristallografiya, 15, 1067-1068.

Ra, H.S., Ok, K.M., and Halasyamani, P.S. (2003) Combining Second-order Jahn-Teller distorted cations to create highly efficient SHG materials: Synthesis, characterization, and NLO properties of BaTeMO (M = Mo or W). Journal of the American Chemical Society, 125, 7764-7765.

Richter, P.W., Kruger, G.J., and Pistorius, C.W.F.T. (1976) $PbWO_4$-III (a high-pressure form). Acta Crystallographica, B32, 928-929.

Rivezzi, N., and Sciau, P. (1998) Etude de la solution solide entre tungstate et tellurate de magnesium: $Pb_2MgW_xTe_{(1-x)}O_6$. Journal of Solid State Chemistry, 139, 332-341.

Robinson, K., Gibbs, G.V., and Ribbe, P.H. (1971) Quadratic Elongation: A Quantitative Measure of Distortion in Coordination Polyhedra. Science, 172, 567–570.

Shannon, R.D. (1976) Revised effective ionic radii and systematic studies of interatomic distances in halides and chalcogenides. Acta Crystallographica, A32, 751–767.

Shaw, R., and Claringbull, G.F. (1955) X-ray study of raspite (monoclinic $PbWO_4$). American Mineralogist, 40, 933.

Sheldrick, G.M. (2008). A short history of SHELX. Acta Crystallographica, A64, 112-122.

Takai, S., Sugiura, K., and Esaka, T. (1999) Ionic conduction properties of $Pb_{1-x}M_xWO_{4+\delta}$ (M = Pr, Tb). Materials Research Bulletin 34, 193-202.

Tyson, R.M., Hemphill, W.R., and Theisen, A.F. (1988) Effect of the W:Mo ratio on the shift of excitation and emission spectra in the scheelite-powellite series. American Mineralogist, 73(9-10), 1145-1154.

Always consult and cite the final, published document. See http://www.minsocam.org or GeoscienceWorld

Revision 1

Wang, L., Bian, J.J., and Guo, G.H. (2010) Phase transition and microwave dielectric properties of LiY($W_{1-x}Te_x$)2O8 ($0.0 \leq x \leq 0.2$). Materials Chemistry and Physics, 124, 748-750.

Yang, X., and Huang, J. (2012) Phase transformation of lead tungstate at normal temperature from tetragonal structure to monoclinic structure. Journal of the American Ceramic Society, 95, 3334-3338.

Yeom, T.H., and Lim, A.R. (2012) Magnetic resonance studies on ^{207}Pb nuclei and paramagnetic impurities in $PbWO_4$:Eu, $PbWO_4$:Gd, and pure $PbWO_4$ single crystals. Journal of Molecular Structure, 1027, 44–48.

Zhang, Y., Holzwarth, N.A.W., and Williams, R.T. (1998) Electronic band structures of the scheelite materials $CaMoO_4$, $CaWO_4$, $PbMoO_4$, and $PbWO_4$. Physical Review B, 57, 12738.

Zheng, C., Hu, C., Chen, X., Xiong, Y., Xu, J., Wan, B., and Huang, L. (2010) Raspite $PbWO_4$ nanobelts: synthesis and properties. CrystEngComm, 12, 3277-3282.

Always consult and cite the final, published document. See http://www.minsocam.org or GeoscienceWorld

Revision 1

Figure 1. Crystal structure of Te-rich raspite. The octahedra and spheres represent the MO_6 (M = W + Te) groups and Pb atoms, respectively.

Figure 2. Raman spectra of Te-rich and regular raspites at room temperature. The spectra are shown with vertical offset for more clarity.

Figure 3. Raman spectra of regular and Te-rich raspites annealed at different temperatures. The Raman spectrum of stolzite was taken from the RRUFF Project (http://rruff.info/R050568) for comparison. The spectra are shown with vertical offset for more clarity. Annealing temperatures are indicated on the left.

Table 1. Crystallographic data and refinement results for Te-rich and regular raspites

Table 2. Coordinates and displacement parameters of atoms in Te-rich raspite and regular raspite.

Table 3. Selected bond distances and angles for Te-rich and regular raspites.

Always consult and cite the final, published document. See http://www.minsocam.org or GeoscienceWorld

294 **Table 1.** Crystallographic data and refinement results for Te-rich and regular raspites

	Te-rich raspite	**Regular raspite**
Chemical formula	$Pb(W_{0.56}Te_{0.44})O_4$	$PbWO_4$
Crystal size (mm)	$0.05 \times 0.04 \times 0.04$	$0.05 \times 0.05 \times 0.04$
Space group	$P2_1/a$ (No. 14)	$P2_1/a$ (No. 14)
a (Å)	13.621(3)	13.5773(8)
b (Å)	5.0187(12)	4.9806(3)
c (Å)	5.5858(14)	5.5670(3)
β (°)	107.979(5)	107.658(3)
V (Å^3)	363.19(15)	358.72(4)
Z	4	4
ρ_{cal} (g/cm^3)	7.869	8.426
λ (Å)	0.71073	0.71073
μ (mm^{-1})	67.40	78.76
2θ range for data collection	≤65.34	≤65.15
No. of reflections collected	5113	8180
Index ranges	$-20 \le h \le 15$ $-7 \le k \le 7$ $-8 \le l \le 8$	$-20 \le h \le 19$ $0 \le k \le 7$ $0 \le l \le 8$
No. of independent reflections	1336	1315
No. of reflections with $I > 2\sigma(I)$	1211	1156
No. of parameters refined	57	56
R(int)	0.033	0.048
Final R factors [$I > 2\sigma(I)$]	$R_1 = 0.026$, $wR_2 = 0.052$	$R_1 = 0.025$, $wR_2 = 0.053$
Final R factors (all data)	$R_1 = 0.031$, $wR_2 = 0.054$	$R_1 = 0.032$, $wR_2 = 0.055$
Goodness-of-fit	1.13	1.06

295
296

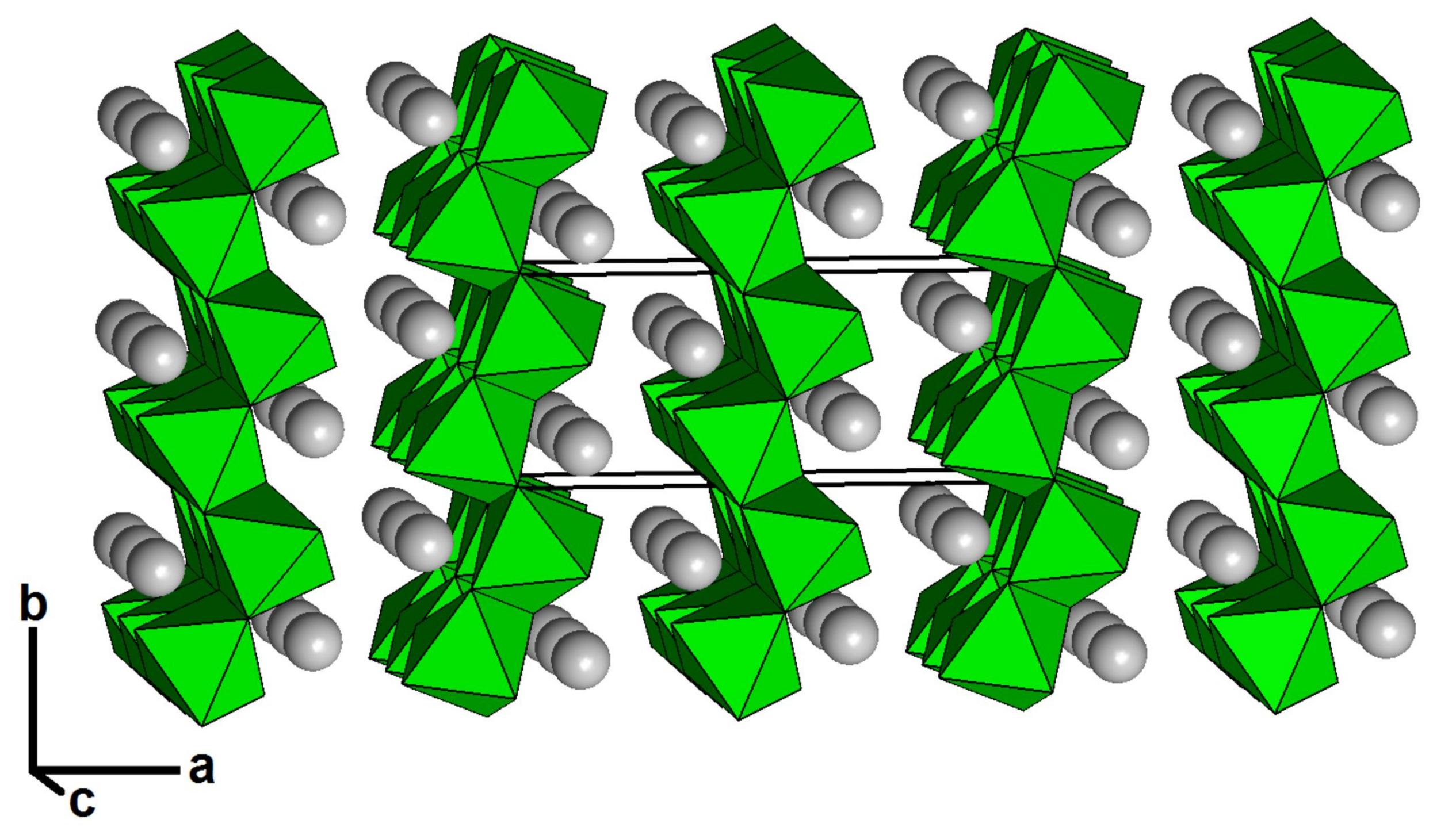
b
a
c

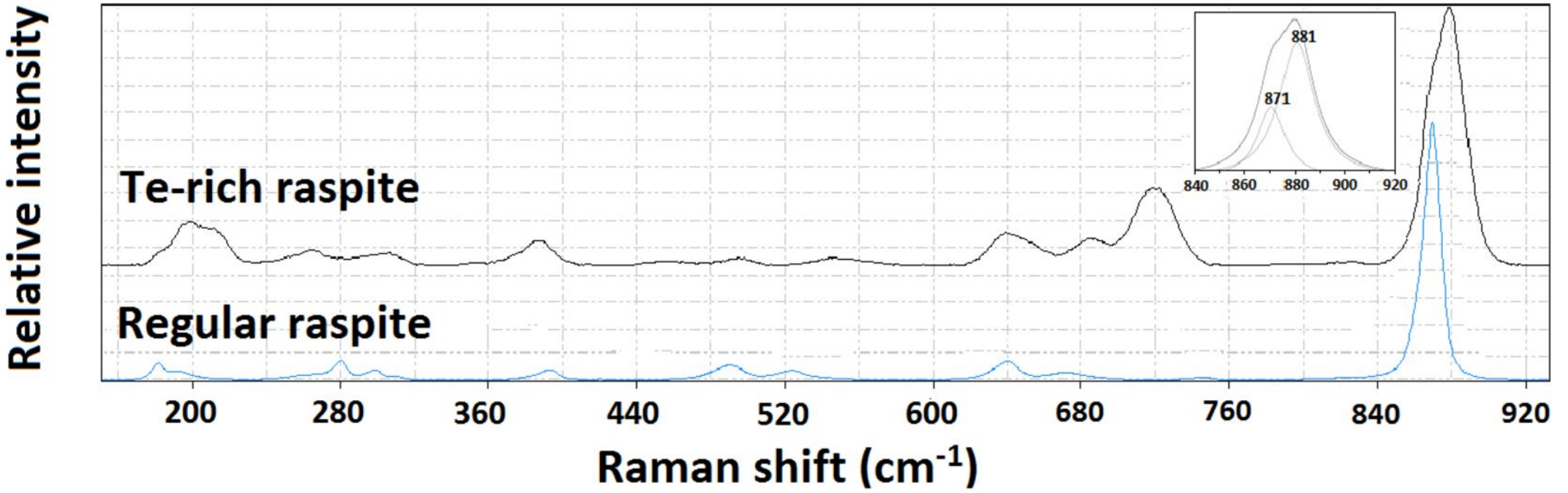
Relative intensity
Te-rich raspite
Regular raspite
881
871
840
860
880
900
920
200
280
360
440
520
600
680
760
840
920
Raman shift (cm-1)

Stolzite

Te-rich raspite (600°C)

Te-rich raspite (580°C)

Regular raspite (400°C)

Regular raspite (390°C)

Relative intensity

200 280 360 440 520 600 680 760 840 920

Raman shift (cm^{-1})

Table 1. Crystallographic data and refinement results for Te-rich and regular raspites

	Te-rich raspite	**Regular raspite**
Chemical formula	$Pb(W_{0.56}Te_{0.44})O_4$	$PbWO_4$
Crystal size (mm)	$0.05 \times 0.04 \times 0.04$	$0.05 \times 0.04 \times 0.03$
Space group	$P2_1/a$ (No. 14)	$P2_1/a$ (No. 14)
a (Å)	13.621(3)	13.5773(8)
b (Å)	5.0187(12)	4.9806(3)
c (Å)	5.5858(14)	5.5670(3)
β (°)	107.979(5)	107.658(3)
V (Å^3)	363.19(15)	358.72(4)
Z	4	4
ρ_{cal} (g/cm^3)	7.869	8.426
λ (Å)	0.71073	0.71073
μ (mm^{-1})	67.40	78.76
2θ range for data collection	≤65.34	≤65.15
No. of reflections collected	5113	8180
No. of independent reflections	1336	1315
No. of reflections with $I > 2\sigma(I)$	1211	1156
No. of parameters refined	57	56
R(int)	0.033	0.048
Final R factors [$I > 2\sigma(I)$]	$R_1 = 0.026$, $wR_2 = 0.052$	$R_1 = 0.025$, $wR_2 = 0.053$
Final R factors (all data)	$R_1 = 0.031$, $wR_2 = 0.054$	$R_1 = 0.032$, $wR_2 = 0.055$
Goodness-of-fit	1.13	1.06

Table 2. Coordinates and displacement parameters of atoms in Te-rich raspite and regular raspite.

Atom	*x*	*y*	*z*	U_{iso}	U_{11}	U_{22}	U_{33}	U_{23}	U_{13}	U_{12}
Te-rich raspite (R130514)										
Pb	0.15739 (2)	0.19923 (6)	0.16068 (6)	0.02070 (9)	0.0182(1)	0.0245(2)	0.0206(2)	-0.0067(1)	0.0078(1)	-0.0008(1)
M	0.07414 (2)	0.75045 (6)	0.59996 (6)	0.01008 (9)	0.0106(1)	0.0080(1)	0.0108(1)	0.0013(1)	0.0020(1)	0.0000(1)
O1	0.0195 (4)	0.0548 (10)	0.7274 (9)	0.0131 (9)	0.0136(22)	0.0147(21)	0.0087(21)	-0.0042(17)	0.0001(17)	0.0031(17)
O2	0.0195 (4)	0.4347 (9)	0.3918 (9)	0.0111 (9)	0.0121(21)	0.0082(19)	0.0162(23)	0.0000(16)	0.0091(18)	0.0002(16)
O3	0.1472 (4)	0.6318 (11)	0.9075 (9)	0.0182 (10)	0.0198(25)	0.0213(25)	0.0093(22)	0.0069(19)	-0.0017(19)	-0.0034(20)
O4	0.1847 (4)	0.8853 (10)	0.5273 (10)	0.0150 (9)	0.0103(22)	0.0186(23)	0.0162(23)	0.0083(19)	0.0043(19)	0.0007(18)
Regular raspite (R050567)										
Pb	0.14961 (2)	0.19458 (6)	0.16665 (5)	0.01241 (9)	0.01146 (14)	0.01554 (15)	0.01123 (14)	−0.00060 (9)	0.00496 (10)	0.00496 (10)
W	0.07711 (2)	0.74936 (5)	0.61164 (5)	0.00792 (8)	0.00726 (14)	0.00834 (14)	0.00809 (14)	0.00048 (9)	0.00222 (10)	0.00222 (10)
O1	0.0172 (4)	0.0442 (11)	0.7282 (10)	0.0117 (10)	0.011 (2)	0.014 (3)	0.009 (3)	−0.0001 (19)	0.002 (2)	0.002 (2)
O2	0.0627 (4)	0.4416 (11)	0.3930 (10)	0.0112 (10)	0.008 (2)	0.012 (2)	0.017 (3)	−0.003 (2)	0.009 (2)	0.009 (2)
O3	0.1468 (4)	0.6191 (12)	0.9101 (10)	0.0155 (11)	0.014 (3)	0.017 (3)	0.015 (3)	0.002 (2)	0.003 (2)	0.003 (2)
O4	0.1865 (4)	0.8922 (11)	0.5388 (10)	0.0135 (11)	0.010 (3)	0.016 (3)	0.016 (3)	0.004 (2)	0.005 (2)	0.005 (2)

Note: M = 0.56 W + 0.44 Te.

Table 3. Selected bond distances and angles for Te-rich and regular raspites**.**

	$Pb(W_{0.56}Te_{0.44})O_4$	$PbWO_4$
W-O1	1.929(5)	1.886 (5)
W-O1’	2.118(5)	2.192 (5)
W-O2	1.941(5)	1.930 (5)
W-O2’	2.080(5)	2.116 (5)
W-O3	1.800(5)	1.767 (6)
W-O4	1.807(5)	1.800 (5)
Average	1.946	1.9450
OV	9.472	9.426
OQE	1.029	1.038
OAV	85.4	104.2
Pb-O1	2.665 (5)	2.663(5)
Pb-O1’	2.958(5)	2.773(6)
Pb-O2	2.412 (4)	2.323 (5)
Pb-O3	2.571 (5)	2.545 (6)
Pb-O3’	2.823(6)	2.946(6)
Pb-O4	2.495 (5)	2.529 (6)
Pb-O4’	2.495 (5)	2.486(5)
Average	2.635	2.610
Polyhedral Volume	24.295	23.923

Note: OV--octahedral volume, OQE--octahedral quadratic elongation, OAV-- octahedral angle variance (Robinson et al., 1971).